

Impact of Wind Forcing, Bottom Topography, and Inertia on Midlatitude Jet Separation in a Quasigeostrophic Model

TAMAY M. ÖZGÖKMEN, ERIC P. CHASSIGNET, AND AFONSO M. PAIVA

RSMAS/MPO, University of Miami, Miami, Florida

(Manuscript received 2 January 1997, in final form 21 April 1997)

ABSTRACT

The persistence of unrealistic Gulf Stream separation in numerical models of the ocean has prompted many theories about possible mechanisms that influence the separation of a western boundary current from the coast. In this paper, the joint effects of (a) coastline orientation, (b) bottom topography, and (c) inertia on the midlatitude jet separation are explored in a wind-driven two-layer quasigeostrophic model. It is shown that topographic effects are of importance in high eddy activity regions and that eddy–topography interactions strongly influence the separation process.

In order for the western boundary current to separate from the coastline and cross the f/h contours associated with the continental rise, eddy fluctuations need to be weak at the separation point. This can be achieved either by introducing a positive wind stress curl in the northern part of the domain or by increasing the inertia of the western boundary current. In both cases, the separation is facilitated by low eddy activity, resulting in a decoupling of the upper layer from the lower layer when the current crosses the f/h contours.

1. Introduction

The North Atlantic Ocean has perennially been the most observed and studied of all the world's oceans. As a result, robust circulation features have become well identified throughout the years. The strongest signature is of course the western boundary current, which, after exiting the Gulf of Mexico via the Florida Straits, follows the coastline northward as the Gulf Stream and then separates from the coast north of Cape Hatteras (35°N) (Stommel 1965). Just after separation, the Gulf Stream's transport increases several times due to the inertial recirculation gyres that form on both flanks of the jet (Hogg and Johns 1995).

Most ocean general circulation models (OGCMs) have great difficulties in reproducing this basic pattern. The modeled Gulf Streams in general have the tendency to separate far north of Cape Hatteras and to form a large stationary anticyclonic eddy at the separation latitude (e.g., Beckmann et al. 1994; Bryan et al. 1995). They also fail to generate the cyclonic recirculation gyre located on the northern side of the observed Gulf Stream (Hogg et al. 1986). This is of importance because an unrealistic representation of the Gulf Stream system is likely to affect the remainder of the modeled North Atlantic circulation. The Gulf Stream region is subject to

some of the highest observed air–sea heat exchange rates in the World Ocean (Hsiung 1985) and any large displacement of the Gulf Stream's axis will have an impact on the modeled thermohaline circulation. Incorrect separation is especially pronounced in coarse-resolution simulations, whereas recent high-resolution simulations performed with MICOM (Miami Isopycnic Coordinate Ocean Model) at 1/12° grid spacing (Bleck et al. 1995) and with the GFDL-MOM (Geophysical Fluid Dynamics Laboratory—Modular Ocean Model) at 1/6° (Chao et al. 1996) show a marked improvement in the separation behavior. These results appear to indicate that highly inertial solutions are needed for a correct separation of the western boundary current.

The persistence of unrealistic Gulf Stream separation in numerical models has prompted many theories regarding the possible mechanisms that influence the separation of a western boundary current from the coast. The early linear, frictional models (e.g., Stommel 1948; Munk 1950) suggest that separation takes place as a result of the change in sign of the wind stress curl. This theory is further supported by the fact that the observed mean path of the Gulf Stream roughly overlies the zero wind stress curl line (ZWCL). The ZWCL, however, shows considerable seasonal variation (e.g., Isemer and Hasse 1987), while the point of separation shows remarkable consistency. Inclusion of the nonlinear terms and associated boundary conditions (no slip or free slip) induces considerable variations in the separation latitude (Cessi 1991; Chassignet and Gent 1991; Haidvogel et al. 1992; Verron and Blayo 1996). Most of these studies,

Corresponding author address: Dr. Tamay M. Özgökmen, RSMAS/MPO, University of Miami, 4600 Rickenbacker Causeway, Miami, FL 33149-1098.
E-mail: tamay@obelix.rsmas.miami.edu

however, do not include any coastline geometry or bottom topography. Separation can be influenced by a change in coastline orientation, as illustrated by Dengg (1993) in a barotropic numerical model, or by a change in bottom topography, as shown by Holland (1973) in a multilayer model. The combined impact of the coastline orientation and bottom topography on separation is an issue that has not yet been sufficiently addressed.

Other mechanisms have been put forth as being important in the separation process, such as outcropping (Parsons 1969; Veronis 1973; Huang and Flierl 1987; Chassignet and Bleck 1993), interaction with the deep western boundary current (Thompson and Schmitz 1989; Spall 1996), surface cooling (Ezer and Mellor 1992; Chassignet et al. 1995; Özgökmen and Cushman-Roisin 1997, manuscript submitted to *J. Phys. Oceanogr.*) and eddy-topography interactions (Holloway 1992). For a comprehensive review of these theories, the reader is referred to Dengg et al. (1996).

In this paper, the sensitivity of midlatitude jet separation to (i) wind forcing, (ii) bottom topography, and (iii) inertia is investigated in a basin with an angled coastline using a two-layer quasigeostrophic numerical model. The layout of the paper is the following: in section 2, some background is presented. The characteristics and parameters of the numerical model are discussed in section 3. The numerical experiments are presented in section 4. First, a series of reference experiments with flat bottom are discussed. Then, an idealized topography representative of a continental rise is incorporated and its impact on the model's solution is investigated. Finally, the influence of inertia on the western boundary current's separation is evaluated. The importance of the wind forcing patterns is investigated by performing parallel experiments with single and double gyre forcing. The results are summarized and discussed in section 5.

2. Background

The remarkable consistency of the Gulf Stream's separation at Cape Hatteras in time and space raises the following question: Is there any control exerted by either the coastline or the topography in that specific region?

The importance of the coastline orientation on the Gulf Stream's separation was recently addressed in a numerical study by Dengg (1993), who demonstrated that the turn of the coastline away from the western boundary current can indeed induce separation, provided that the current is highly inertial and that no-slip boundary conditions are prescribed. The key process was the production of positive relative vorticity along the coast and its subsequent advection to the separation point via nonlinear terms in the barotropic potential vorticity equation. These results were obtained with a barotropic, flat-bottom numerical model.

The importance of bottom topography has been investigated over the years in some detail. The North At-

lantic western boundary current, after flowing over the shallow continental shelf (water depths of less than 1000 m) between the Florida Straits and Cape Hatteras, separates by crossing the continental rise, where the bottom topography drops sharply to 5000 m within a few hundred kilometers (Fig. 1). From a potential vorticity analysis combined with observational considerations, Warren (1963) inferred that the topography of the continental rise was of significant importance in controlling the Gulf Stream's path. In a similar study, Greenspan (1963) also argued that bottom topography exerts a considerable influence on the Gulf Stream's separation from the coastline and on its subsequent meander pattern. In a barotropic numerical study, Holland (1967) concluded that the Gulf Stream's separation, meandering, and transport are strongly related to topographic effects. In a later study, Holland (1973) demonstrated that it was essential to include the effect of stratification when investigating the influence of bottom topography since the bottom torque can be highly modified due to the baroclinicity of the flow (see also Myers et al. 1996).

The impact of a continental slope on the dynamics of a western boundary current was also addressed by Salmon (1992, 1994) by integrating analytically and numerically the planetary geostrophic equations for a two-layer, double-gyre system. Salmon (1994) demonstrated that the low transport values produced by the wind in the subpolar gyre were carried southwestward along the f/h lines to produce a region of southward flow between the coast and the western boundary current of the subtropical gyre. However, the planetary geostrophic equations used by Salmon (1992, 1994) do not incorporate the inertial terms, which are of importance in western boundary currents (e.g., Harrison and Holland 1981).

Recently, Thompson (1995) studied the effect of continental rises in the context of a three-layer quasigeostrophic model. Thompson (1995) considered a symmetrically forced double-gyre circulation with free-slip boundary conditions along the western wall and found that the presence of topography broke the symmetry between the subpolar and subtropical gyres. The mean path of the midlatitude jet was deflected to the north of the ZWCL, while the separation point remained unaffected.

In this paper the joint effects of (i) wind forcing, (ii) bottom topography, and (iii) inertia on the midlatitude jet separation are explored in a two-layer, quasigeostrophic model. This work can be considered as a natural extension of the work of Dengg (1993) and Thompson (1995) to baroclinic flows with bottom topography and angled coastline orientation.

3. The numerical model

The quasigeostrophic model used in this study is similar to the one developed by Holland (1978). The governing equations of the model can be written in non-dimensional form as

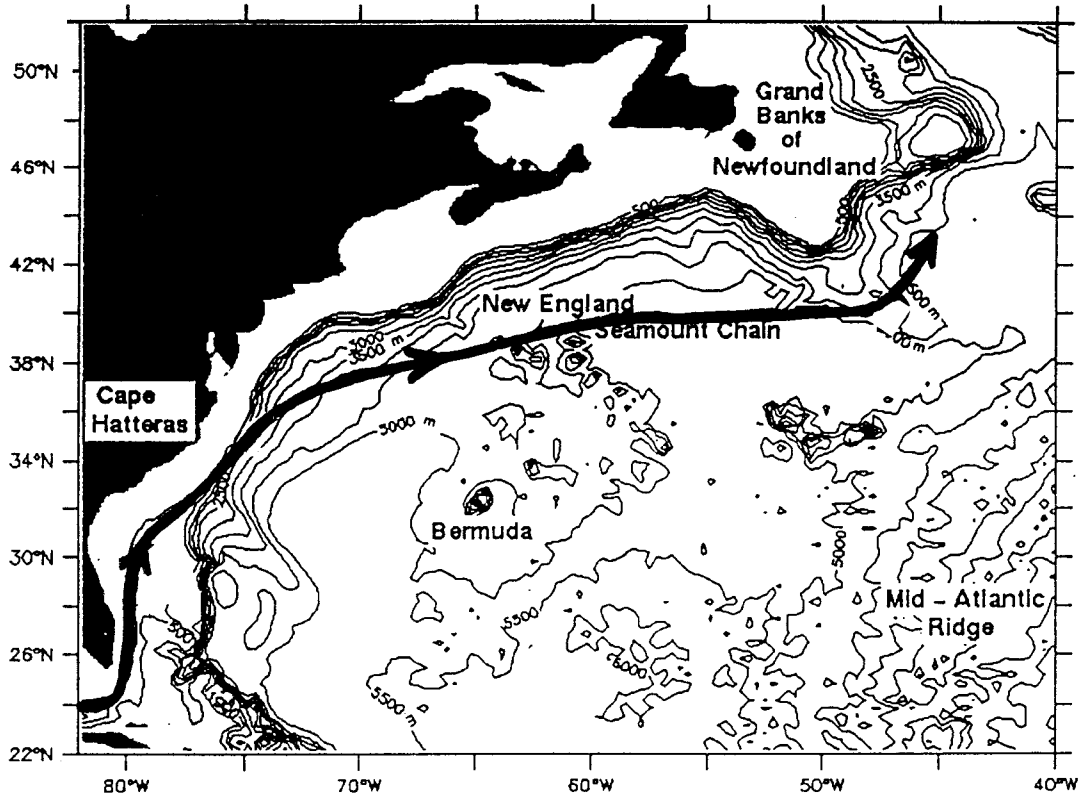


FIG. 1. Bottom topography in the Gulf Stream region. The bold line delineates the mean path of the Gulf Stream. Adapted from Dengg (1996).

$$q_{1t} + J(\psi_1, q_1) = \frac{w_E}{\delta} + A\nabla^4\psi_1 \tag{1}$$

$$q_{2t} + J(\psi_2, q_2) = A\nabla^4\psi_2 - \sigma\nabla^2\psi_2, \tag{2}$$

where q_1 and q_2 are the upper- and lower-layer potential vorticities given by

$$q_1 = y + \frac{F}{\delta}(\psi_2 - \psi_1) + R\nabla^2\psi_1 \tag{3}$$

$$q_2 = y + \frac{F}{1 - \delta}(\psi_1 - \psi_2) + R\nabla^2\psi_2 + \frac{f_0}{\beta l(1 - \delta)} \frac{b}{H}, \tag{4}$$

and ψ_1 and ψ_2 are the upper- and lower-layer stream-functions defined as

$$\psi_1 = \frac{\beta H}{f_0^2 W l} \left(g' \eta + \frac{p}{\rho_0} \right)$$

and

$$\psi_2 = \frac{\beta H}{f_0^2 W l} \frac{p}{\rho_0}, \tag{5}$$

where $w_E(x, y)$ is the Ekman pumping distribution, W its amplitude, l the domain length scale, $p(x, y, t)$ the

lower-layer pressure, h_0 the upper-layer depth scale, $\eta(x, y, t)$ the interface displacement (positive downward), H the total domain depth scale, $b(x, y)$ the bottom topography height (positive upward), g' the reduced gravity, ρ_0 the reference (upper layer) density, f_0 the Coriolis frequency at a reference latitude, β the meridional gradient of the Coriolis frequency, ν the lateral viscosity coefficient, and r the bottom friction coefficient. The nondimensional parameters are defined as the layer ratio $\delta = h_0/H$, the basin Rossby number $R = f_0 W / \beta^2 H^2 = V/\beta l$, the Froude number $F = f_0^2 W / g' \beta^2 H^2$, the lateral friction parameter $A = \nu/\beta l$, and the bottom friction parameter $\sigma = r/\beta l$, where $V = f_0 W / \beta H$ is the barotropic Sverdrup velocity scale.

The prognostic equations (1) and (2) are advanced in time using a predictor-corrector type leapfrog method (Gazdag 1976). The Jacobian operator $J(a, b) = a_x b_y - a_y b_x$ is computed using the formulation proposed by Arakawa (1966) that conserves kinetic energy and enstrophy and satisfies the antisymmetric property $J(a, b) = -J(b, a)$. The diagnostic equations (3) and (4) are inverted using a relaxation method.

Potential vorticity budgets of the various experiments are performed to analyze the dynamical response of the model to changes in forcing and configuration (see the appendix for details). For a typical potential vorticity analysis, the reader is referred to Harrison and Holland

(1981) and Boudra and Chassignet (1988). The influence of bottom topography can be discussed to some extent by computing the topographic stretching due to the bottom flow (TOPO in the appendix). This term,

$$J\left(\overline{\psi}_2, \frac{b}{H}\right) = J\left(\overline{\psi}_B, \frac{b}{H}\right) - \delta J\left(\overline{\psi}_1 - \overline{\psi}_2, \frac{b}{H}\right), \quad (6)$$

where $\overline{\psi}_B = \delta\overline{\psi}_1 + (1 - \delta)\overline{\psi}_2$ is the time-averaged barotropic streamfunction and $\overline{\psi}_1 - \overline{\psi}_2$ the time-averaged baroclinic streamfunction, can be expressed as the difference between the topographic stretching associated with the barotropic flow and a baroclinic “correction” term that represents the joint effect of baroclinicity and bottom relief (or the JEBAR term, cf. Mertz and Wright 1992).

4. The numerical experiments

The numerical model is configured in a domain with a zonal length of 3000 km and a meridional length of 2000 km corresponding to the latitudinal extent 22°–40°N. A simplified coastline is incorporated as a wedge-shaped boundary with a sharp kink located at 35°N, hereafter referred to as the cape. No-slip boundary conditions are applied along the western boundary. A viscous sublayer with a vorticity of opposite sign from that of the interior flow is generated and advected along the boundary, thereby providing favorable conditions for a separation of the western boundary current from the coastline. Free-slip boundary conditions, on the other hand, do not generate such a viscous sublayer, so that the current tends to follow the coastline (Boudra and Chassignet 1988; Dengg 1993). Following the recommendations of Verron and Blayo (1996), the second-order scheme of Woods (1954) was implemented for the no-slip boundary condition. Free-slip boundary conditions are applied at all remaining boundaries. The lateral friction coefficient is determined by the grid spacing (20 km) and is equal to 200 m² s⁻¹. Other parameters common to all experiments are the bottom friction coefficient $r = 2 \times 10^{-7}$ s⁻¹, the upper-layer depth $h_0 = 1000$ m, the total depth $H = 5000$ m, and the reduced gravity $g' = 0.02$ m s⁻² (corresponding internal radius of deformation ≈ 43 km). Interactions with surrounding flows [subpolar gyre, deep western boundary current (DWBC), equatorial system, etc.] are suppressed as no-flow conditions are imposed on all boundaries. The numerical model is integrated for 5 to 10 years after each parameter change until the basin-integrated kinetic and available potential energies reach a statistically steady state. The model is then run for an additional 5 years to calculate the time-averaged flow patterns.

In this section, the influence of coastline orientation, bottom topography, and inertia is systematically investigated. First, in 4a, the impact of several wind stress distributions on the jet's separation latitude is discussed in a series of flat bottom experiments. The importance

TABLE 1. In all experiments, the domain size is 3000 km by 2000 km in zonal and meridional directions, respectively. The domain is centered around 35°N. The grid spacing is equal to 20 km in both directions. The experiments share the common bottom friction coefficient $r = 2 \times 10^{-7}$ s⁻¹, lateral viscosity $\nu = 200$ m² s⁻¹, upper-layer depth scale $h_0 = 1000$ m, total fluid depth scale $H = 5000$ m, and reduced gravity $g' = 0.02$ m s⁻² (internal radius of deformation ≈ 43 km). They differ in wind forcing and bottom topography as listed above. The superscript (*) indicates a 100% increase in the amplitude of wind stress forcing from the previous experiment.

| Expt | Wind | Topography |
|------|------|------------|
| I | W1 | — |
| II | W2 | — |
| III | W3 | — |
| IV | W4 | — |
| V | W2 | B1 |
| VI | W2* | B1 |
| VII | W1* | B1 |
| VIII | W3* | B1 |
| IX | W4 | B1 |
| X | W4 | B2 |

of bottom topography and inertia is then investigated in 4b. The parameters for the experiments are given in Table 1.

a. Influence of wind stress distribution and coastline orientation—Flat bottom experiments

Most available climatologies [Leetma and Bunker 1978; Hellerman and Rosenstein 1983; Isemer and Hasse 1987; COADS (Comprehensive Ocean–Atmosphere Data Set, e.g., Mayer and Weisberg 1992)] show that the observed path of the Gulf Stream roughly follows the annual mean ZWCL. They also all display a positive wind stress curl north of the Gulf Stream. The corresponding Sverdrup transports, however, differ substantially among the climatologies. In Hellerman and Rosenstein (1983), Isemer and Hasse (1987), and COADS, the Sverdrup circulation is anticyclonic over the subtropical gyre and gradually decreases from a maximum at the center of the gyre to values of 5–10 Sv (Sv $\equiv 10^6$ m³ s⁻¹) north of Cape Hatteras. On the other hand, in Leetmaa and Bunker (1978), the positive wind stress curl north of the Gulf Stream is strong enough to reverse the sign of the Sverdrup flow north of the Gulf Stream axis and drive a cyclonic flow of approximately 5–10 Sv.

To quantify the importance of these differences on the midlatitude jet separation, the impact of several idealized wind forcing patterns is investigated in some detail. First, in the experiments of section 4a(1), the wind stress is zonal with varying meridional structure and is such that the corresponding Sverdrup circulation is anticyclonic everywhere. Then, in the experiments of section 4a(2), the wind forcing pattern is modified to include a positive wind stress curl north of Cape Hatteras that is strong enough to drive a cyclonic flow in the northern part of the domain.

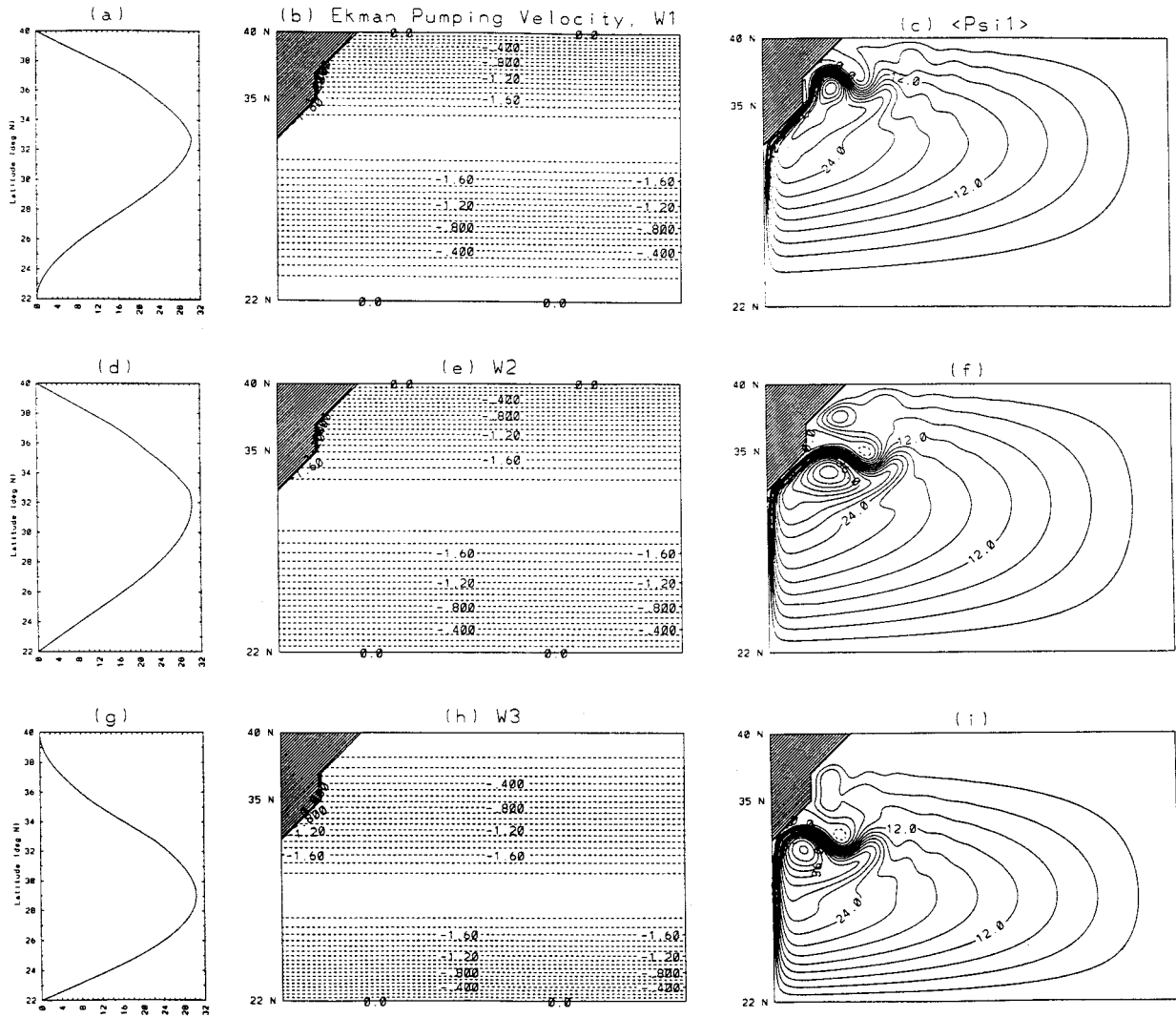


FIG. 2. (a, d, g) The Sverdrup transport along the western boundary, and (b, e, h) the Ekman pumping velocity ($CI = 0.1 \times 10^{-6} \text{ m s}^{-1}$) resulting from the wind stress distributions W1, W2, and W3, respectively. The corresponding upper-layer transport streamfunctions ($CI = 3 \text{ Sv}$) for experiments I, II, and III are depicted in (c, f, i). The angle brackets indicate time-averaged mean component.

1) SINGLE GYRE FORCING—EXPERIMENTS I–III

Three experiments (expts I–III) are presented in this section to illustrate the sensitivity of the western boundary current separation latitude to the meridional structure of the wind forcing. The results are summarized in Fig. 2. In all three experiments, the wind stress distribution is purely zonal (Figs. 2b,e,h) and the resulting circulation is anticyclonic. The amplitude of the wind forcing is such that it generates a maximum transport of about 30 Sv along the western boundary, which is approximately of the order of the observed mean Florida Current transport (Schmitz and Richardson 1968). The wind forcing is quasi symmetric in the meridional direction in experiment II (W2), is intensified to the north in experiment I (W1), and is intensified to the south in experiment III (W3) (Figs. 2b,e,h) (Table 1). The north–south migration of the maximum wind stress curl line

from W1 to W3 is about 400 km and falls within the observed seasonal migration of wind forcing over the North Atlantic Ocean (Isemer and Hasse 1987). In all experiments, the ocean depth is a uniform 5000 m.

Despite similarities in the wind stress distributions in these experiments, the resulting upper-layer time-averaged mean streamfunctions display a large degree of variability in the separation latitude of the western boundary current. In experiment II, the western boundary current follows the coastline east at 35°N before separating at the sharp change in coastline representing Cape Hatteras (Fig. 2f). The eastward penetration distance of the jet is relatively small and, shortly after separation, the jet bifurcates. Most of the flow recirculates south and enhances the subtropical recirculation gyre. A small portion bifurcates northward and forms a recirculation gyre before connecting with the Sverdrup

interior flow. While experiment II exhibits separation at the cape (35°N), the variations in the position of the maximum wind stress curl in experiments I and III significantly modify the resulting circulation. In experiment III, the western boundary current separates before reaching the cape (Fig. 2i), whereas in experiment I, the western boundary current does not appear to be strongly influenced by the presence of the coastline geometry. The current in experiment I follows the coastline northward all the way to the northern boundary despite the abrupt changes in the coastline orientation (Fig. 2c).

These results show some conceptual similarity to those obtained by Cessi (1991) in the context of a limited-area barotropic model with a straight coastline. Cessi's model was configured such that the inflow profiles of two (colliding) western boundary currents and an exit profile were specified. As in the present study, the separation latitude of the colliding western boundary currents is sensitive to the characteristics and to the meridional placement of the exit profile. A modification of the meridional structure of the wind forcing essentially changes the latitude of the exit conditions for the midlatitude jet. We have performed additional experiments (not illustrated) that explored the impact of the tilt and zonal structure in the wind forcing pattern; no significant changes in the separation latitude were observed.

The sensitivity of the separation latitude to wind forcing was also recognized by Dengg (1993) and the results presented in this section are in qualitative agreement with the results of several of his experiments, despite the fact that he used a barotropic model. This is not too surprising since the circulation in our two-layer simulations is mostly confined to the upper layer. The lower layer is set in motion through eddy momentum fluxes generated by the instabilities of the midlatitude jet so that most of the lower layer flow is located near the jet. The mean signature of the mesoscale eddies consists of recirculating gyres of the same sign in both layers. However, one would expect significant differences from simulations performed with a barotropic model once bottom topography is included [inclusion of the JEBAR, Eq. (6)].

2) DOUBLE GYRE FORCING—EXPERIMENT IV

The impact of double gyre forcing ($W4$) (Table 1) is investigated by incorporating a positive wind stress curl north of Cape Hatteras (Fig. 3a), strong enough to force a cyclonic gyre with a transport of the order of 10–15 Sv (Figs. 3b,c). The ZWCL is also slightly tilted to the north in order to blend the influence of negative and positive wind stress curls as suggested by the available climatologies (see section 4a).

The upper-layer streamfunction for experiment IV (flat bottom) is displayed in Fig. 3d. The primary difference from the single gyre experiments is in the emergence of a cyclonic circulation at the northwest corner of the domain, driven by the positive wind stress curl.

The disconnection of this gyre from the separation point indicates that the cyclonic forcing has a “passive” role in the separation process. The western boundary current separates near the cape, and the separation latitude is primarily dictated by the meridional structure of the wind forcing as in the single gyre experiments. Sensitivity experiments (not illustrated) showed that the tilt in the wind forcing axis does not strongly influence the separation latitude.

b. Influence of wind stress distribution and coastline orientation—Experiments with bottom topography

The importance of a continental rise on midlatitude jet separation and path has been pointed out by several studies (Holland 1967, 1973; Salmon 1992, 1994; Thompson 1995). To quantify its importance in the context of the numerical simulations of 4a, bottom topography representative of the continental rise is added and its impact on western boundary current separation is discussed in this section as a function of wind stress distribution, inertia, and stratification.

1) SINGLE GYRE FORCING—EXPERIMENTS V–VIII

(i) Impact of bottom topography B1

The flat bottom experiment experiment II is chosen as the reference experiment for experiment V (Table 1) since (i) the wind forcing $W2$ is quasi-symmetric and (ii) the western boundary current separates at the sharp coastline bend. The idealized bottom topography (B1) used in experiment V consists of a smooth and gradual rise of 1000 m toward the continent and a plateau on the western boundary before the sharp turn in coastline orientation at 35°N (Fig. 4a). The corresponding f/h contours for the lower layer are displayed in Fig. 4b. The total variation of topography is small enough, with respect to the depth of the lower layer, for the quasi-geostrophic approximation to remain valid.

The results for experiment V are displayed in Fig. 5a. In this experiment, the western boundary current no longer separates at the cape as in the flat bottom experiment II (Fig. 2f) but instead follows the coastline northward forms a stationary anticyclonic eddy, and then separates from the coast. This pattern is strongly reminiscent of surface fields simulated by a far more complex primitive equation numerical model (GFDL Community Modeling Experiment; Bryan et al. 1995) (Fig. 5b). Despite the fact that the models differ greatly in terms of sophistication (primitive equations, monthly thermodynamic forcing, 30 levels for the GFDL model), the flow patterns along the western boundary and near the separation point are very similar. This aspect is emphasized by the overlay in Fig. 5b of the simplified configuration used for the quasigeostrophic simulations.

To analyze experiment V in more detail, the time-averaged transport streamfunctions and vorticities (rel-

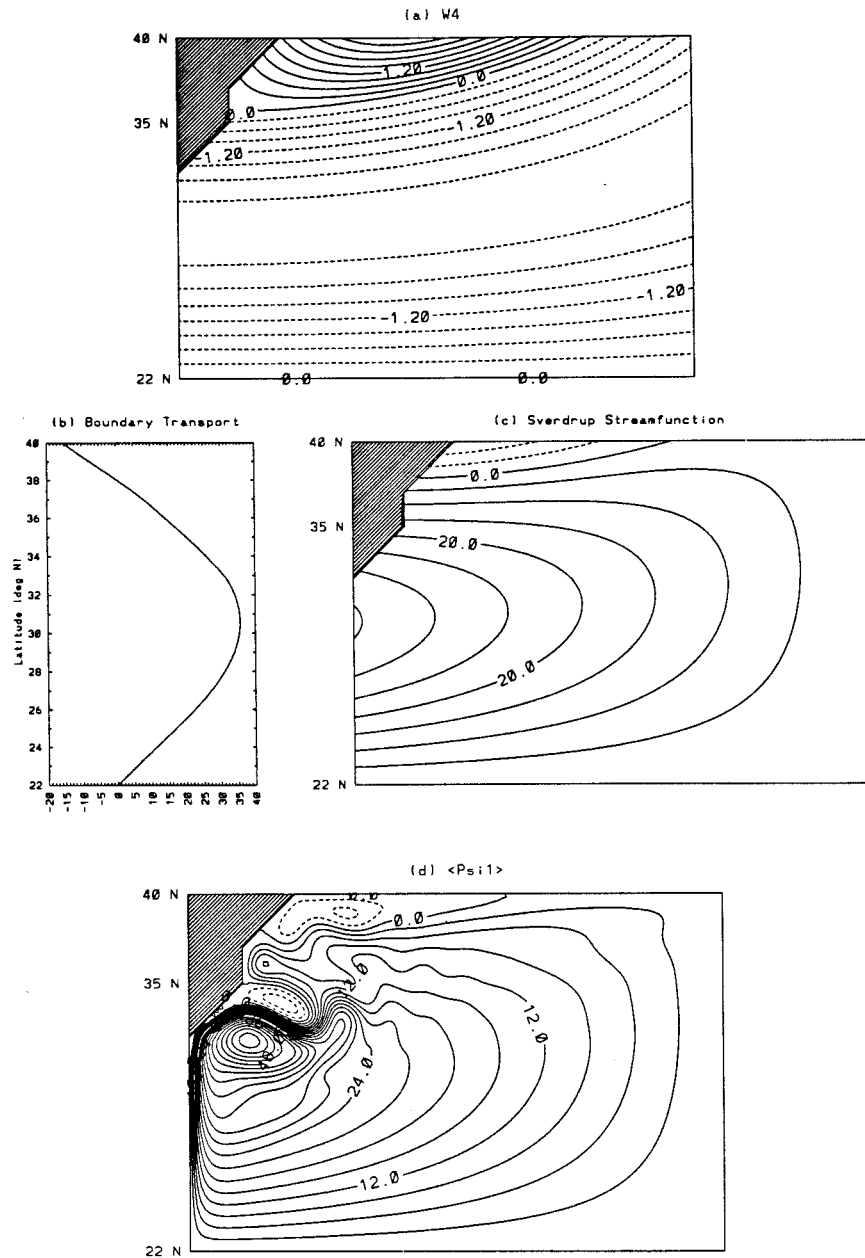


FIG. 3. (a) The Ekman pumping velocity ($CI = 0.3 \times 10^{-6} \text{ m s}^{-1}$), (b) Sverdrup transport along the western boundary (in Sv), and (c) Sverdrup streamfunction ($CI = 5 \text{ Sv}$) associated with the wind stress distribution W4. (d) Resulting upper-layer mean flow ($CI = 3 \text{ Sv}$) for experiment IV.

ative and potential) of both layers near the separation point are displayed in Fig. 6. The corresponding potential vorticity budgets (see the appendix for details) and spatial distribution of eddy kinetic energy are shown in Figs. 7 and 8 for the upper and lower layer, respectively. The stationary anticyclonic eddy possesses a strong barotropic component (Figs. 6b,e,h) and can consequently affect the upper-layer flow through interactions with the bottom topography. However, the lower-layer potential vorticity contours (Fig. 6f) are not strongly influenced

by this stationary eddy and are mostly dominated by the bottom topography. Both the upper layer and the barotropic relative vorticity contours (Figs. 6a,g) show that the flow tends to follow the f/h contours (Fig. 4b) and cannot cross them (Fig. 6i).

In the absence of direct forcing, the lower layer is set in motion through eddy momentum fluxes generated by instabilities. Topographic stretching (TOPO) will then be generated, provided that a mean flow is established in the lower layer via the fluctuations. Feedback to the

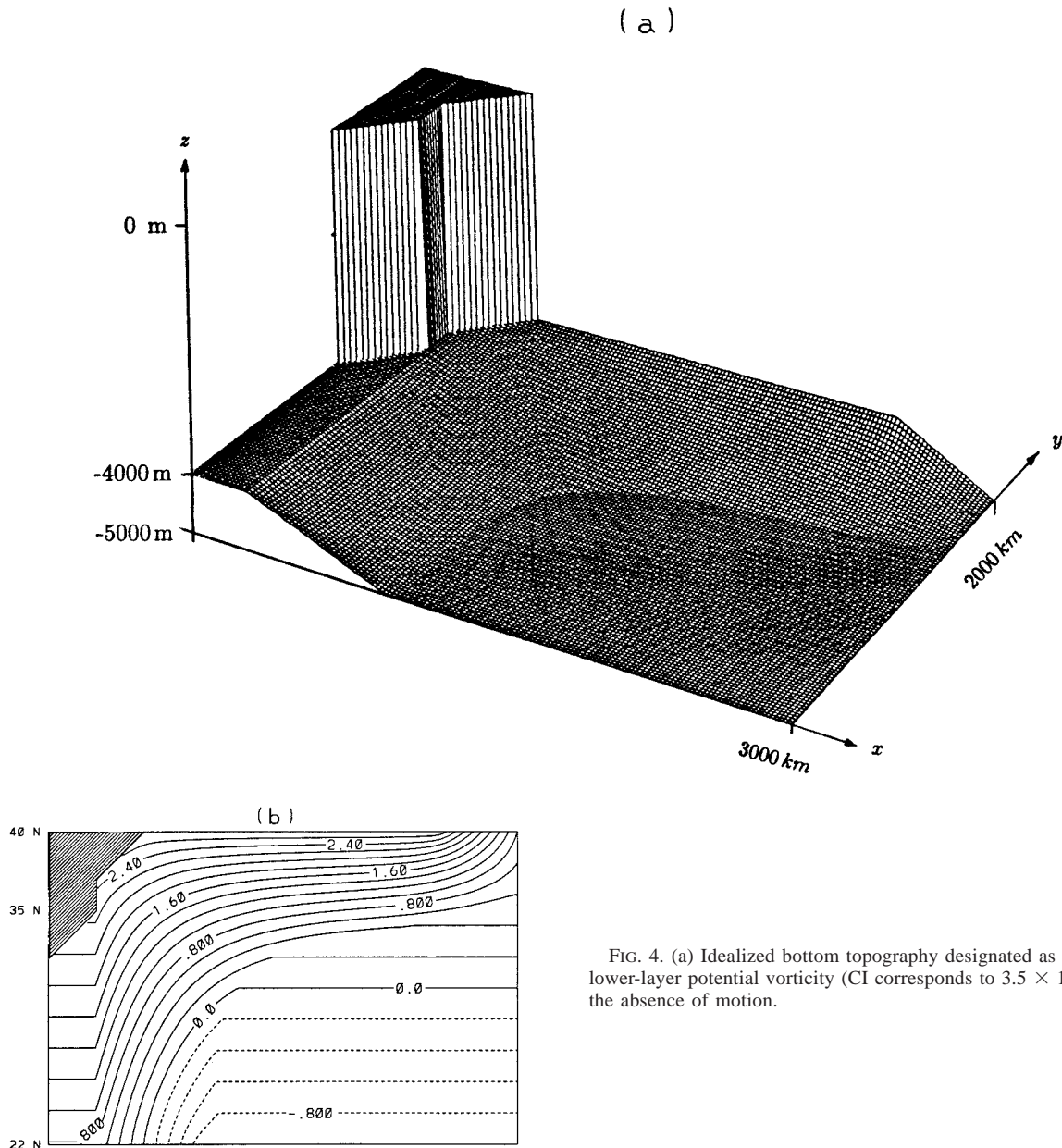


FIG. 4. (a) Idealized bottom topography designated as *B1* and (b) lower-layer potential vorticity (*CI* corresponds to $3.5 \times 10^{-6} \text{ s}^{-1}$) in the absence of motion.

upper layer will then be established via vortex stretching (STRCH). In other words, topographic effects will be felt by the upper layer in high eddy activity regions. The magnitude of this eddy-induced topographic stress can indeed be significant (Holloway 1992).

In experiment V, the main balance in the upper layer (Fig. 7) is between planetary and relative vorticity advection (BETA and RVA) with a significant contribution from stretching (STRCH) in the stationary eddy. The contribution from STRCH is representative of high topographic interactions in that region as illustrated by TOPO (Fig. 8d). At the separation point, eddy fluctuations (Figs. 7d, 9e) are high, the jet feels the topography

strongly and, consequently, is unable to cross the f/h contours (Fig. 4b). In the following section, it will be shown that higher inertia in the solution minimizes that effect.

(ii) *Impact of inertia*

One of the primary issues associated with western boundary currents in numerical ocean models is their highly viscous nature. This is especially pronounced in basin and global simulations where the grid spacing is, at best, marginal to resolve the current profile and therefore the corresponding viscosity must be quite high.

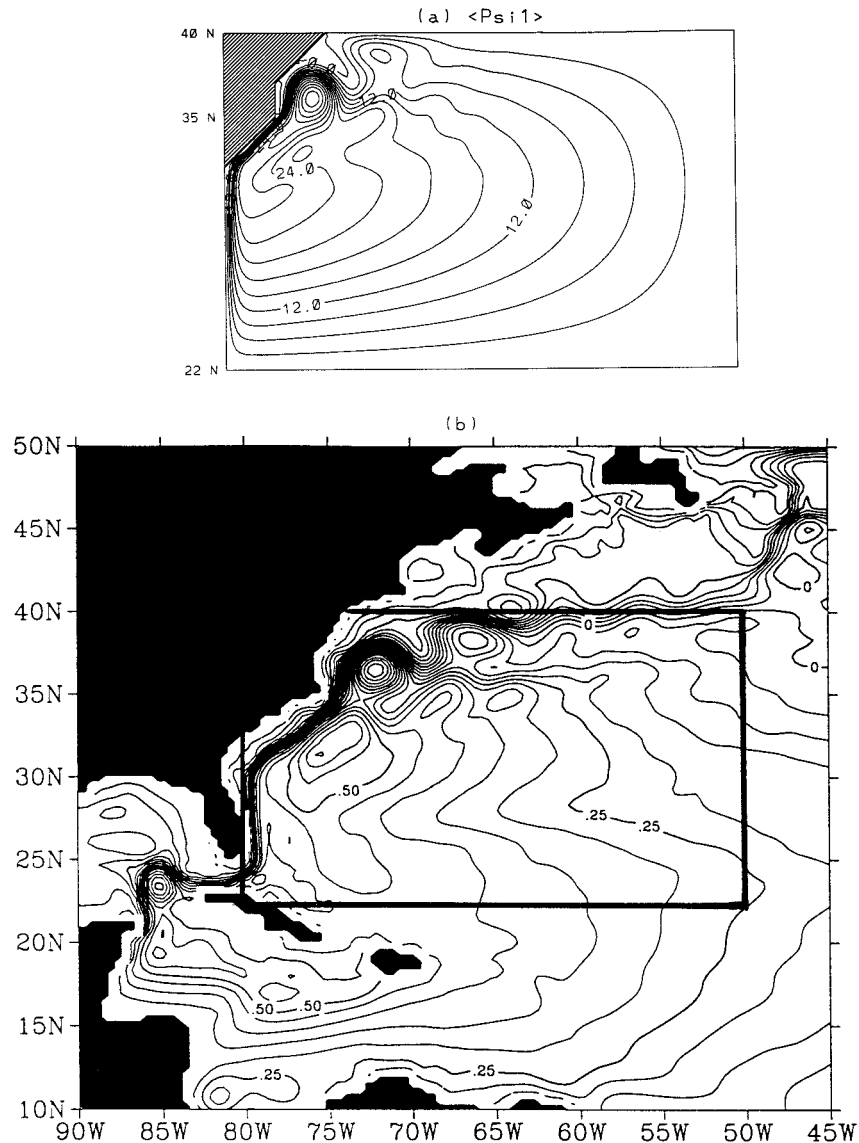


FIG. 5. (a) Upper-layer transport streamfunction ($CI = 3$ Sv) for experiment V, which is driven by wind forcing W2 and incorporates topography B1. (b) Surface pressure distribution ($CI = 0.05$ decibars) from a $1/3^\circ$ CME simulation (Bryan et al. 1995). The solid line marks the corresponding boundary of the present idealized configuration.

However, western boundary currents are highly inertial, and it has been argued that most of the energy dissipation in the Gulf Stream system is actually achieved in the recirculating gyres via bottom friction (Weatherly 1984). A misrepresentation of the dynamical balance in simulated western boundary currents is therefore likely to jeopardize the processes that take place downstream, such as the process of separation.

In the present eddy-resolving model, which has a relatively higher horizontal resolution ($20 \text{ km} \approx 1/6^\circ$ at midlatitudes) than most basin-scale primitive equation experiments (typically $1/3^\circ$ – 1°), the topographic effects appear to dominate the separation process, even though

the bottom topography is not as steep as in reality. Recent high-resolution simulations, however, performed with MICOM (Miami Isopycnic Coordinate Ocean Model) at $1/12^\circ$ grid spacing (Bleck et al. 1995) and with the GFDL-MOM (Geophysical Fluid Dynamics Laboratory—Modular Ocean Model) at $1/6^\circ$ (Chao et al. 1996) have shown a marked improvement in the separation behavior, and these results appear to indicate that highly inertial solutions are needed for a correct separation.

In order to quantify how inertial a western boundary current is, it is useful to introduce some characteristic scales. In the linear limit, for weak forcing or large

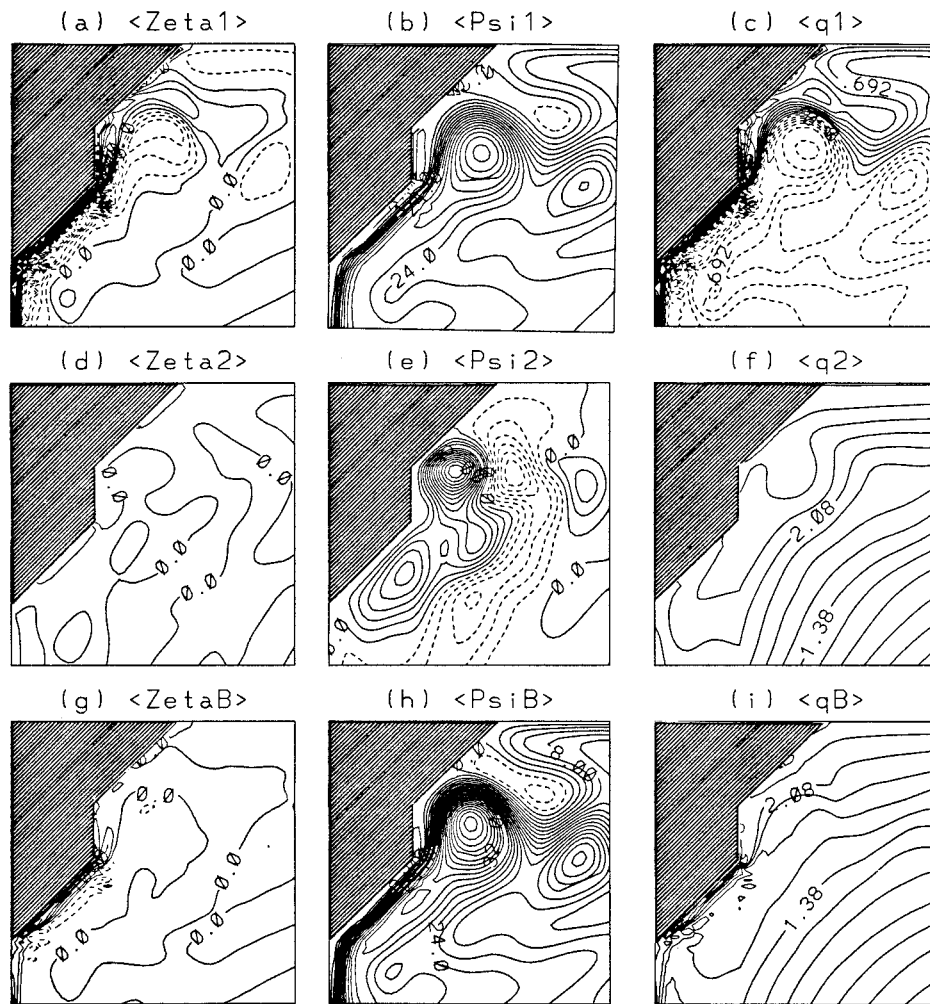


FIG. 6. (a) Upper-layer relative vorticity (CI corresponds to $1.5 \times 10^{-6} \text{ s}^{-1}$), (b) upper-layer transport streamfunction (CI = 3 Sv), (c) upper-layer potential vorticity (CI corresponds to $3 \times 10^{-6} \text{ s}^{-1}$), (d) lower-layer relative vorticity (CI corresponds to $1.5 \times 10^{-6} \text{ s}^{-1}$), (e) lower-layer transport streamfunction (CI = 0.5 Sv), (f) lower-layer potential vorticity (CI corresponds to $3 \times 10^{-6} \text{ s}^{-1}$), (g) barotropic relative vorticity (CI corresponds to $1.5 \times 10^{-6} \text{ s}^{-1}$), (h) barotropic streamfunction (CI = 2 Sv), and (i) total vorticity (CI corresponds to $3 \times 10^{-6} \text{ s}^{-1}$) for experiment V.

viscosity, the boundary layer thickness is given by the Munk scale

$$\delta_v = \left(\frac{\nu}{\beta}\right)^{1/3}. \tag{7}$$

In the nonlinear limit, for strong forcing or small viscosity, the boundary layer thickness is given by the inertial scale

$$\delta_l = \left(\frac{V_1}{\beta}\right)^{1/2}, \tag{8}$$

where $V_1 = f_0 W / \beta H$ is the upper-layer Sverdrup velocity scale. The ratio of the inertial to the viscous boundary layer thickness is then expressed, in terms of dimensional parameters, as

$$\frac{\delta_l}{\delta_v} = D \frac{W^{1/2}}{\nu^{1/3}}, \tag{9}$$

where $D = f_0^{1/2} / (\beta^{2/3} h_0^{1/2})$. For the western boundary current to be considered “inertial,” the ratio δ_l / δ_v must be larger than unity. Since D is set by the model’s configuration, the ratio can be increased either by decreasing the horizontal viscosity coefficient ν or by increasing the amplitude of Ekman pumping W . In experiment V, the ratio $\delta_l / \delta_v = 1.30$ indicates that the solution is not highly inertial. In experiment VI (Table 1), the ratio δ_l / δ_v is increased to 1.84 by imposing an Ekman pumping 100% higher than in experiment V. This was deemed to be more efficient computationally, since a decrease in viscosity would have also required an increase in resolution.

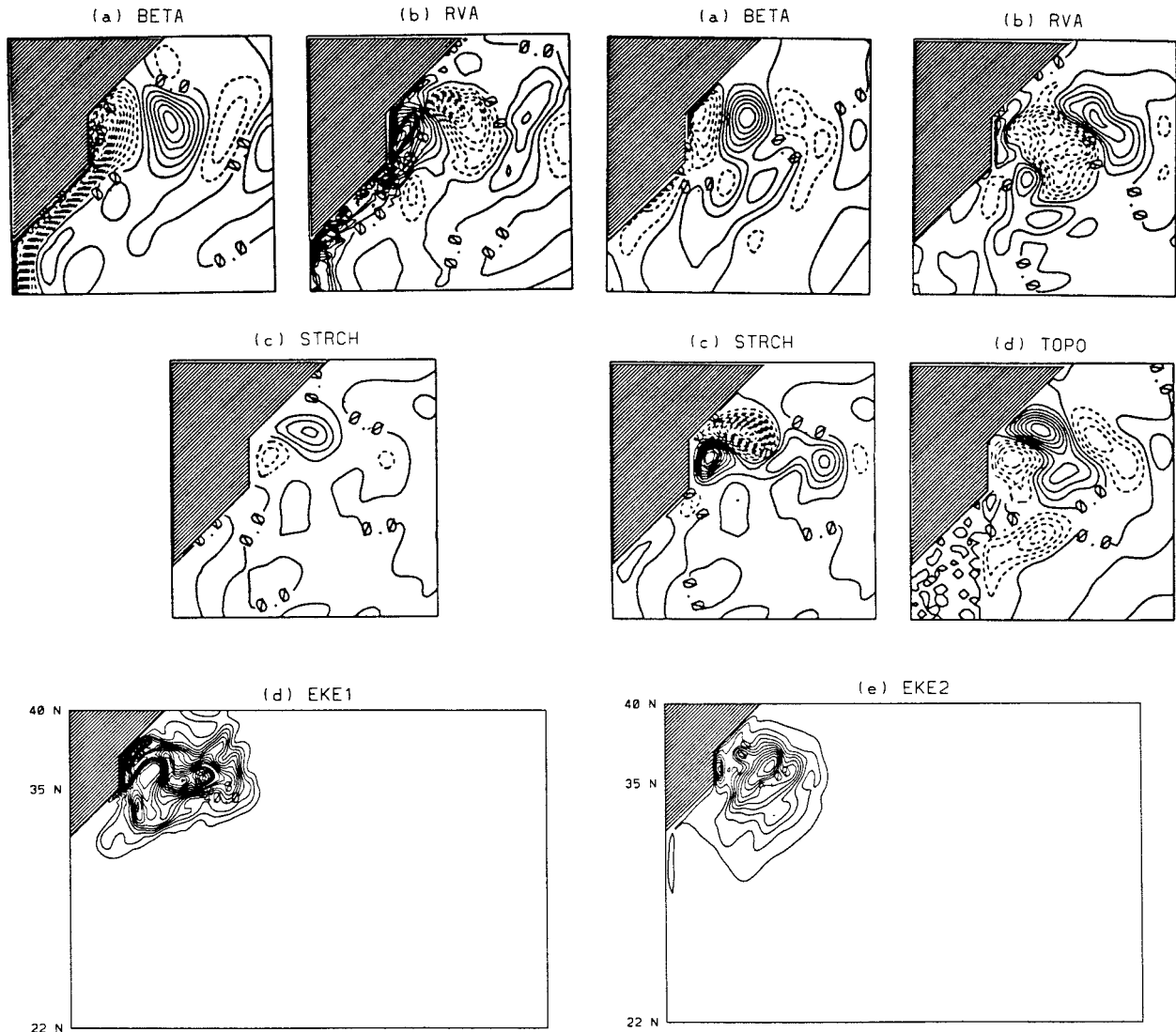


FIG. 7. Contributions of (a) BETA, (b) RVA, and (c) STRCH to the upper-layer potential vorticity budget in the separation region for experiment V (CI corresponds to $7.8 \times 10^{-13} \text{ s}^{-2}$). Contributions of wind forcing and bottom friction are small. Lateral friction is not plotted. (d) Upper-layer eddy kinetic energy (CI = $10 \text{ cm}^2 \text{ s}^{-2}$).

FIG. 8. Contributions of (a) BETA, (b) RVA, (c) STRCH, and (d) TOPO to the lower-layer potential vorticity budget in the separation region for experiment V (CI corresponds to $0.5 \times 10^{-13} \text{ s}^{-2}$). Contributions of bottom and lateral friction are small. (e) Lower-layer eddy kinetic energy (CI = $0.5 \text{ cm}^2 \text{ s}^{-2}$).

The upper-layer time-averaged streamfunction field for experiment VI is displayed in Fig. 9. The upper-layer streamfunction exhibits two new features when compared to that of experiment V. First, the western boundary current separates from the coast at the cape, represented by the sharp corner at 35°N , but also penetrates farther east than in the flat bottom experiments (Fig. 2). Second, a cyclonic gyre forms north of the jet despite that the wind forcing in this region acts in the opposite direction (anticyclonic). This gyre is therefore not directly wind driven but results from the eddies formed by the meandering jet after separation.

As for experiment V, the time-averaged transport streamfunctions and vorticities (relative and potential) of

both layers near the separation point are displayed in Fig. 10. The corresponding potential vorticity budgets are shown in Figs. 11 and 12 for the upper and lower layer, respectively. Contrary to experiment V, both the upper layer and the barotropic relative and potential vorticity contours (Figs. 10a,c,g,i) show that the flow is now able to cross the f/h contours (Fig. 4b). The positive vorticity generated within the viscous sublayer is advected along the boundary and far into the interior (Figs. 10a,g), thereby providing favorable conditions for the separation of the western boundary current as discussed by Boudra and Chassignet (1988) and Dengg (1993).

One of the main differences between experiment VI and the less inertial experiment V is illustrated by the

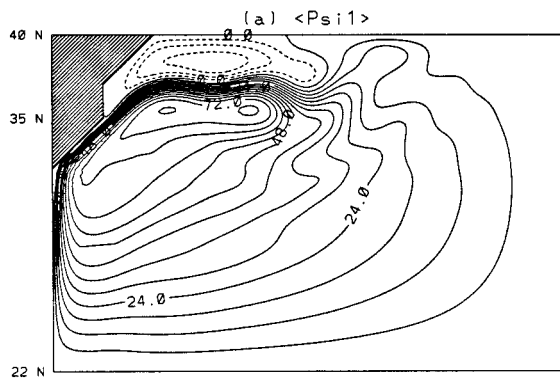


FIG. 9. Upper-layer transport streamfunction ($CI = 6 Sv$) for experiment VI, where the amplitude of Ekman pumping is increased by 100%.

potential vorticity budgets and by the spatial distribution of eddy kinetic energy near the separation point (Figs. 11, 12). Contrary to experiment V, the upper-layer flow in experiment VI does not strongly feel the topography near the separation point, as indicated by the weak stretching (STRCH) (Fig. 11). As in experiment V, the contribution from STRCH is representative of the eddy activity in that region and associated topographic interactions as illustrated by the eddy kinetic energy plots (Figs. 11d, 12e) and TOPO (Fig. 12d). These are minimal over the continental rise and become important only in the meandering jet, which is located farther offshore than in experiment V. In other words, higher inertia facilitates the separation by decoupling the upper layer from the lower layer when the current crosses the f/h contours. Eddy activity (Figs. 11d, 12e), and consequently topographic interactions, is small in experi-

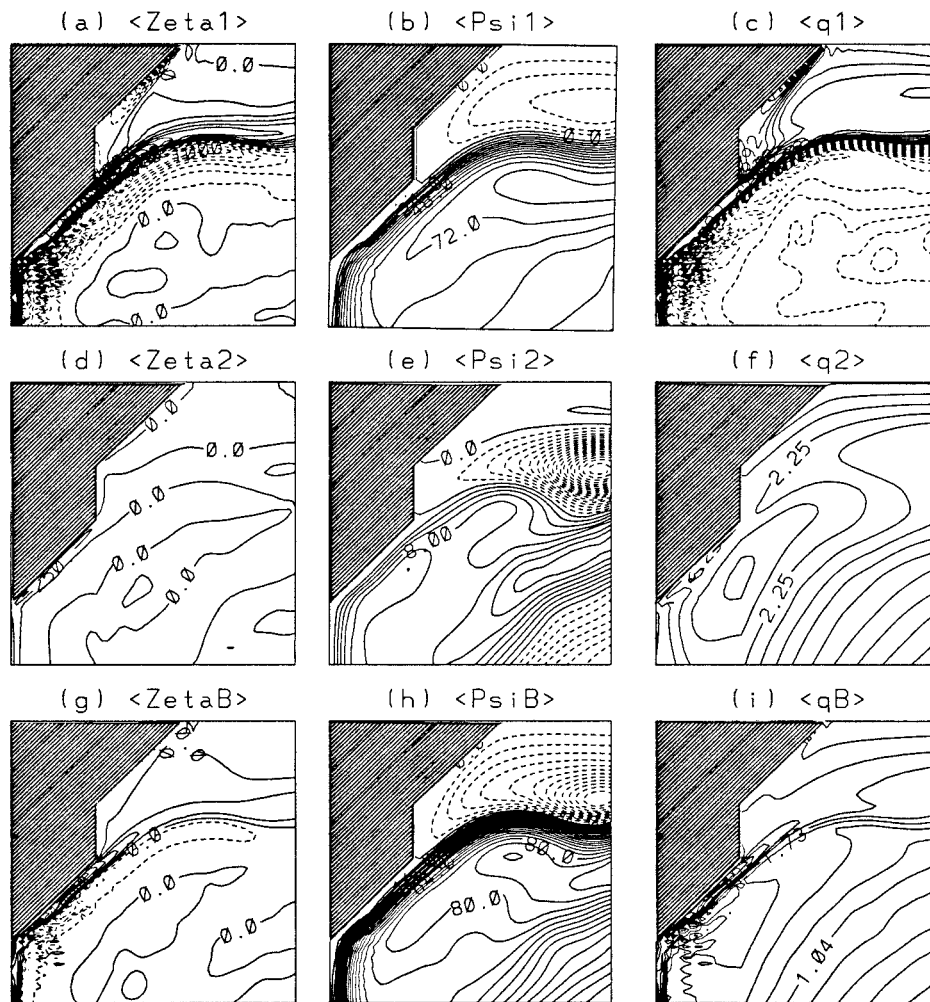


FIG. 10. (a) Upper-layer relative vorticity (CI corresponds to $1.5 \times 10^{-6} s^{-1}$), (b) upper-layer transport streamfunction ($CI = 6 Sv$), (c) upper-layer potential vorticity (CI corresponds to $3 \times 10^{-6} s^{-1}$), (d) lower-layer relative vorticity (CI corresponds to $1.5 \times 10^{-6} s^{-1}$), (e) lower-layer transport streamfunction ($CI = 2 Sv$), (f) lower-layer potential vorticity (CI corresponds to $3 \times 10^{-6} s^{-1}$), (g) barotropic relative vorticity (CI corresponds to $1.5 \times 10^{-6} s^{-1}$), (h) barotropic streamfunction ($CI = 4 Sv$), and (i) total vorticity (CI corresponds to $3 \times 10^{-6} s^{-1}$) for experiment VI.

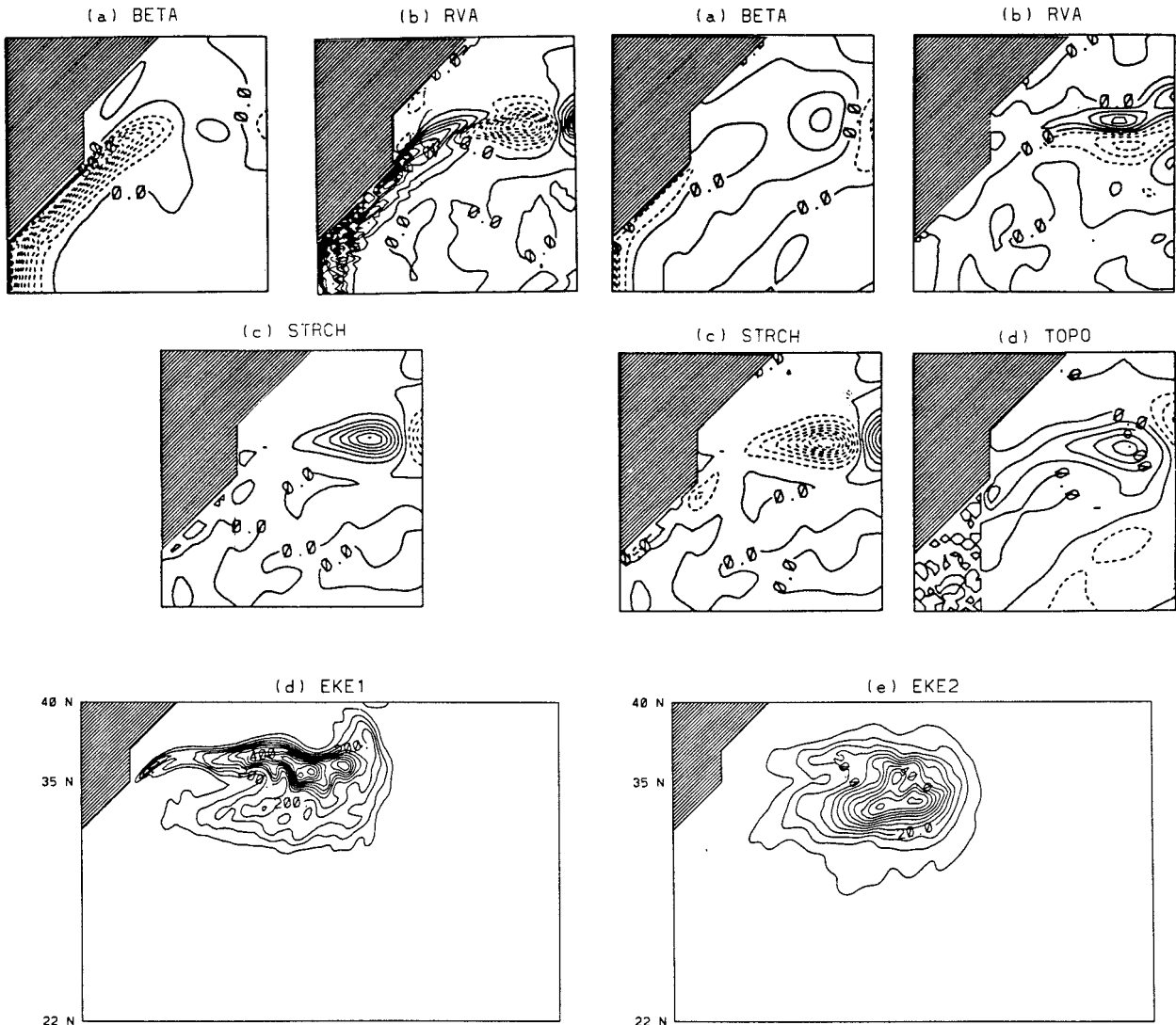


FIG. 11. Contributions of (a) BETA, (b) RVA, and (c) STRCH to the upper-layer potential vorticity budget in the separation region for experiment VI (CI corresponds to $15.2 \times 10^{-13} \text{ s}^{-2}$). (d) Upper-layer eddy kinetic energy (CI = $50 \text{ cm}^2 \text{ s}^{-2}$).

FIG. 12. Contributions of (a) BETA, (b) RVA, (c) STRCH, and (d) TOPO to the lower-layer potential vorticity budget in the separation region for experiment VI (CI corresponds to $3.1 \times 10^{-13} \text{ s}^{-2}$). (e) Lower-layer eddy kinetic energy (CI = $5 \text{ cm}^2 \text{ s}^{-2}$).

ment VI as the jet moves away from the coastline over the steep topography.

Since the observed wind stress patterns exhibit considerable latitudinal movements over a 1-yr period (e.g., Isemer and Hasse 1987), while the observed point of separation shows remarkable consistency, one may ask if the separation observed in the highly inertial experiment VI is actually sensitive to the position of the maximum wind stress curl as was the case in the flat bottom experiments (experiments I–III). To investigate that question, two experiments (experiments VII and VIII) (Table 1) were performed with the wind stress distributions W1 and W3 of section 4a and, as in experiment VI, with an Ekman pumping 100% higher than in the corresponding flat bottom experiments (experiments I

and III). The upper-layer mean flows of these two experiments are displayed in Fig. 13. Despite the large latitudinal variation of 400 km in the position of the maximum wind stress curl between experiments VII and VIII, the midlatitude jet separates in both experiments at the cape (35°N). The path of the jet once separated, however, does vary as a function of the maximum wind stress curl latitude. In this series of experiments, highly inertial flows appear to be a necessary factor for a realistic separation process, with the coastline geometry controlling the separation latitude.

(iii) On the role of stratification

Modification of the stratification can counteract, through the JEBAR term [Eq. (6)], the barotropic to-

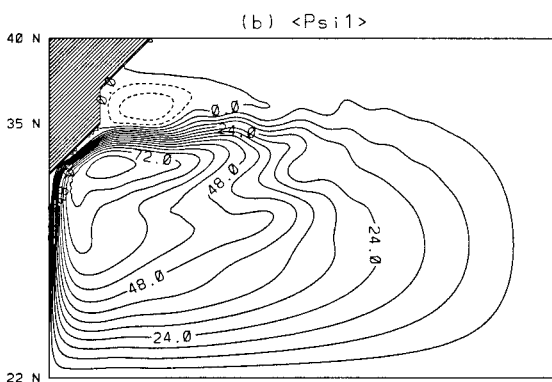
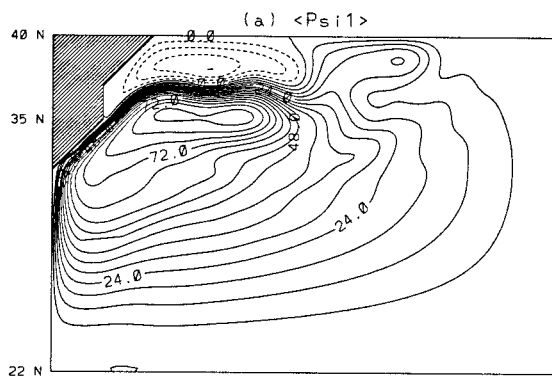


FIG. 13. Upper-layer transport streamfunctions ($CI = 6 \text{ Sv}$) for (a) experiment VII driven by wind forcing $W1^*$ (same as $W1$ but twice the amplitude of forcing) and (b) experiment VIII driven by wind forcing $W3^*$ (same as $W3$ but twice the amplitude of forcing). Both experiments include bottom topography $B1$.

pographic steering. This steering plays a significant role in experiment V, and a strong JEBAR term may be able to significantly reduce the torque induced by the barotropic component. In the limit of strong stratification, the layers become uncoupled and the effect of topography should become minimal. Stratification was therefore modified in a series of experiments (otherwise identical to experiment V) by increasing the reduced gravity g' . The resulting flow patterns (not illustrated) do not differ greatly from the base experiment experiment V, even for high values of g' such as 0.1 m s^{-2} (corresponding radius of deformation of more than 100 km). In the context of this two-layer quasigeostrophic model, stratification does not appear to be a controlling factor in the separation process.

2) DOUBLE GYRE FORCING—EXPERIMENTS IX–X

(i) Impact of bottom topography $B1$

When the bottom topography $B1$ is incorporated in the double gyre experiment (wind forcing $W4$, expt IX, Table 1), the flow pattern is considerably modified (Fig. 14) when compared to that of the flat bottom experiment

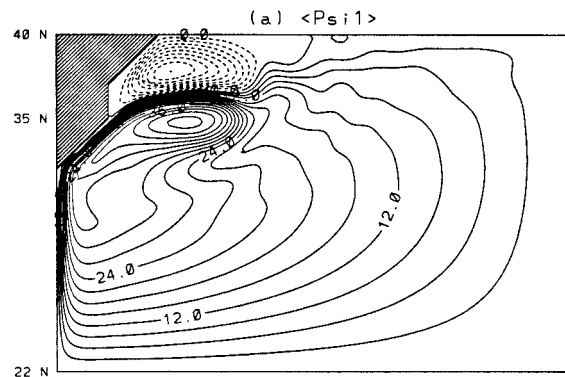


FIG. 14. (a) Upper-layer transport streamfunction ($CI = 3 \text{ Sv}$) for experiment IX, which is driven by wind forcing $W4$ and includes bottom topography $B1$.

IV (Fig. 3d). The midlatitude jet clearly separates from the coast and its penetration distance increases significantly (Fig. 14). The jet also exhibits well-developed recirculations on both flanks. The overall picture is very similar to that of the highly inertial experiment (expt VI) (Fig. 9). The mechanisms for the separation differ, however, since in experiment IX the cyclonic wind forcing plays a significant role and is no longer “passive.” In contrast to the corresponding flat bottom experiment (expt IV) (Fig. 3d), the wind forcing contributes significantly to the driving both of the northern recirculating gyre and of the southward-flowing western boundary current that opposes the overshooting of the northward-flowing current seen in experiment IV (Fig. 3d). In the highly inertial experiment (expt VI), on the other hand, the northern gyre is driven by the meandering jet. Experiment IX also shows that, unlike the flat bottom cases of Dengg (1993) and experiment IV, the inclusion of a cyclonic wind forcing north of the cape combined with topography does significantly modify the jet’s separation process.

As in the highly inertial experiment (expt VI) (Fig. 10), the upper-layer stretching (STRCH) in experiment IX is negligible when compared to the planetary and relative vorticity advections (BETA and RVA) (Fig. 15). As in experiment VI, this reflects minimal topographic interactions as the jet crosses the continental rise. The southward-flowing western boundary current that opposes the overshooting of the northward-flowing current appears to be instrumental in minimizing the eddy activity of the jet as it separates.

(ii) Impact of bottom topography $B2$

The idealized bottom topography $B1$ used in the previous experiments has a weak slope and is marginally representative of the continental slope region. The topographic variations associated with the observed continental shelf break are much greater and cannot be accurately represented within the assumptions of the qua-

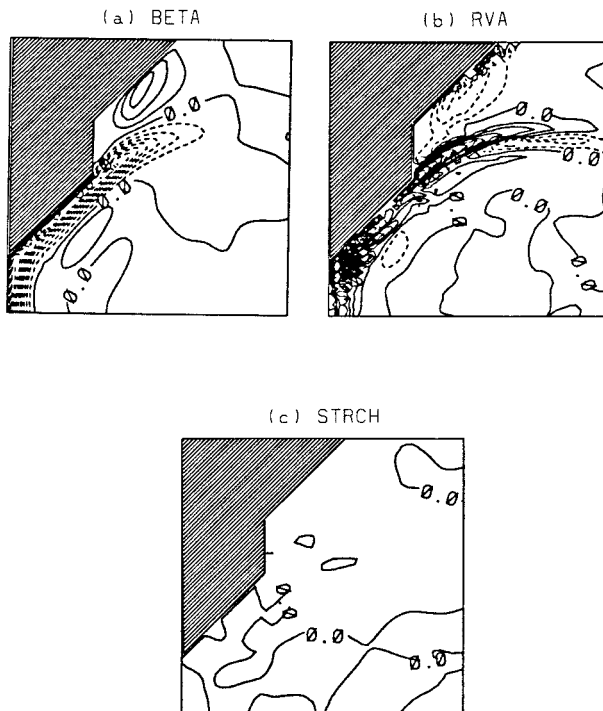


FIG. 15. Contributions of (a) BETA, (b) RVA, and (c) STRCH to the upper-layer potential vorticity budget in the separation region for experiment IX (CI corresponds to $7.8 \times 10^{-13} \text{ s}^{-2}$).

quasigeostrophic model. However, in an attempt to investigate the model's sensitivity to topography, an experiment (expt X) (Table 1) was performed with a topography B2 that differs from B1 by (i) a higher extent (2000 m) and (ii) the superposition of narrow and steep regions along the western and northern boundaries representing the continental shelf break. The variation in height of B2 is smaller than the lower-layer depth and the quasigeostrophic assumption is marginally violated. The flow patterns (not illustrated) do not differ significantly when compared to those of experiment IX (Fig. 14).

5. Summary and discussion

The persistence of unrealistic Gulf Stream separation in numerical models has prompted many theories about possible mechanisms that influence the separation of a western boundary current from the coast. In this paper, the joint effects of (i) wind forcing, (ii) bottom topography, and (iii) inertia on the midlatitude jet separation have been explored in a basin with an angled coastline using a two-layer quasigeostrophic model. This work can be considered as a natural extension of the works of Dengg (1993) and Thompson (1995) to baroclinic flows with bottom topography and coastline orientation. A simplified coastline was incorporated as a wedge-shaped boundary with a sharp turn, located at 35°N , representing Cape Hatteras. The bottom topography

consists of a smooth and gradual rise of 1000 m toward the continent and of a plateau on the western boundary south of the sharp turn in coastline orientation at 35°N . The bottom topography used in this study is idealized and greatly reduced in height and slope due to the limitations of the quasigeostrophic model.

The sensitivity of the separation latitude to the meridional structure of the wind stress distribution was first investigated in a series of experiments with flat bottom. The wind stress distribution was varied to represent characteristic patterns as well as various climatologies (single gyre or double gyre). In all cases, the separation latitude was found to be strongly dependent upon the position of the maximum wind stress curl. Inclusion of the idealized bottom topography in the single gyre experiments significantly modified the upper-layer flow pattern by forcing the western boundary to follow the f/h contours and to overshoot the flat bottom separation latitude.

In the absence of direct forcing (i.e., deep western boundary current, buoyancy forcing, . . .), the lower layer is set in motion through eddy momentum fluxes generated by instabilities. Topographic stretching is then generated, provided that a mean flow is established in the lower layer via the fluctuations. Feedback to the upper layer will then be established via vortex stretching. In other words, topographic effects will be felt by the upper layer in high eddy activity regions. If eddy fluctuations are high at the separation point, then the jet feels the topography strongly and, consequently, is unable to cross the f/h contours.

Two factors were found that minimize the impact of the topographic stress (Holloway 1992) near the separation point. The first one is the inclusion of a positive wind stress curl in the northern part of the domain. In this double gyre experiment, the wind forcing contributes significantly to the driving both of the northern recirculating gyre and of the southward-flowing western boundary current that opposes the overshooting of the northward-flowing current. In the corresponding flat bottom experiment, the jet separated at a lower latitude and the northern gyre played only a passive role. The upper-layer vortex stretching is negligible and corresponds to minimal topographic interactions as the jet crosses the continental rise. The southward-flowing western boundary current that opposes the overshooting of the northward-flowing current appears to be instrumental in minimizing the eddy activity of the jet as it separates.

The second factor is high inertia. In the single gyre experiments, a doubling of the wind stress magnitude also showed that a western boundary current can cross the f/h contours provided that it is highly inertial. High positive relative vorticity is generated within the viscous sublayer adjacent to the boundary and is advected offshore, thereby facilitating the separation process (Boudra and Chassignet 1988; Dengg 1993) and the f/h contour crossing. Contrary to the results of the flat bottom

experiments, once inertial effects dominated, the separation latitude was no longer found to be sensitive to the wind stress distribution. The path of the jet, however, once separated, does depend on the wind stress distribution. In this series of experiments, highly inertial flows appear to be a necessary factor for a realistic separation process, with the coastline geometry controlling the separation latitude. As in the double gyre experiment with topography, the eddy-topography interactions are minimal over the continental rise and become important only in the meandering jet region. Higher inertia facilitates the separation by decoupling the upper layer from the lower layer when the current crosses the f/h contours.

Since most of the climatologies used in realistic simulations do not induce a strong cyclonic gyre (see section 4a) north of 35°N, inertia is likely to be one of the dominant factors required for a realistic separation. This conclusion is supported by recent high-resolution simulations performed with primitive equation numerical models, which show a marked improvement in the separation behavior (Bleck et al. 1995; Chao et al. 1996). Despite the simplicity of the model used in this study, the similarity between the overshooting jet in experiment V and the GDFL Community Modeling Experiment (resolution of 1/3°) (Bryan et al. 1995), and the improvement in the separation in both of the cases (expt VI and Chao et al. 1996) when higher inertia was introduced (by stronger forcing or by higher resolution, respectively), further confirm this assertion.

Many other factors, not taken into account in this study, affect midlatitude jet separation (atmospheric cooling, deep western boundary current, etc.). Finally,

we mention that advection of relative vorticity generated in the boundary layer has been shown to play a significant role in the separation process (Boudra and Chassignet 1988; Dengg 1993), and consequently a proper treatment of the boundary layer is of importance in numerical simulations, especially with coarse resolution. As shown by Verron and Blayo (1996), subgrid-scale parameterization of the vorticity at the wall, to represent the lack of resolution of the boundary layer physics, can lead to a significant improvement in western boundary current separation.

Acknowledgments. The authors wish to thank C. Rooth, M. Spall, and J. Verron for constructive discussions and L. Smith for substantial help in improving the text. Support was provided by the Office of Naval Research under Contract NOOO14-93-1-0404 and by the National Science Foundation under Grant OCE-94-06663. AMP was supported by the Brazilian Research Council (CNPq).

APPENDIX

Potential Vorticity Budget

In order to calculate the potential vorticity budgets, the prognostic variables are decomposed as $\psi = \bar{\psi} + \psi'$, where $\bar{\psi}$ refers to the time-averaged or mean component defined as $\bar{\psi} = T^{-1} \int_{t_0}^{t_0+T} \psi dt$, and ψ' denotes the fluctuating or eddy component such that $\overline{\psi'} = T^{-1} \int_{t_0}^{t_0+T} \psi' dt = 0$. The integration period T must be large compared to the period of the fluctuations. Then, Eq. (3) and (4) can be written as

$$\begin{aligned} \overline{q_{1r}} = & - \underbrace{F[J(\bar{\psi}_1, \bar{\psi}_2) + \overline{J(\psi'_1, \psi'_2)}]}_{\text{STRCH}} / \delta - \underbrace{R[J(\bar{\psi}_1, \nabla^2 \bar{\psi}_1) + \overline{J(\psi'_1, \nabla^2 \psi'_1)}]}_{\text{RVA}} - \underbrace{\bar{\psi}_{1x}}_{\text{BETA}} + \underbrace{\frac{w_E}{\delta}}_{\text{WIND}} + \underbrace{A \nabla^4 \bar{\psi}_1}_{\text{VISC}} \\ \overline{q_{2r}} = & \underbrace{F[J(\bar{\psi}_1, \bar{\psi}_2) + \overline{J(\psi'_1, \psi'_2)}]}_{\text{STRCH}} / (1 - \delta) - \underbrace{R[J(\bar{\psi}_2, \nabla^2 \bar{\psi}_2) + \overline{J(\psi'_2, \nabla^2 \psi'_2)}]}_{\text{RVA}} - \underbrace{\bar{\psi}_{2x}}_{\text{BETA}} \\ & - \underbrace{\frac{f_0}{\beta l (1 - \delta)} J\left(\bar{\psi}_2, \frac{b}{H}\right)}_{\text{TOPO}} + \underbrace{A \nabla^4 \bar{\psi}_2}_{\text{VISC}} - \underbrace{\sigma \nabla^2 \bar{\psi}_2}_{\text{BOTF}}. \end{aligned}$$

The statistically steady state is defined such that $\overline{q_{1r}} = \overline{q_{2r}} = 0$. The individual terms are

- WIND vorticity input by wind forcing
- BETA planetary vorticity advection
- STRCH vortex stretching
- TOPO topographic stretching
- RVA relative vorticity advection

- VISC vorticity dissipation by lateral friction
- BOTF vorticity dissipation by bottom friction.

REFERENCES

Arakawa, A., 1966: Computational design for long-term numerical integration of the equations of fluid motion: Two dimensional incompressible flow. Part I. *J. Comput. Phys.*, **1**, 119–143.

- Beckmann, A., C. W. Böning, C. Köberle, and J. Willebrand, 1994: Effects of increased horizontal resolution in simulations of the North Atlantic Ocean. *J. Phys. Oceanogr.*, **24**, 326–344.
- Bleck, R., S. Dean, M. O'Keefe, and A. Sawdey, 1995: A comparison of data-parallel and message-passing versions of the Miami Isopycnic Coordinate Ocean Model (MICOM). *Parallel Comput.*, **21**, 1695–1720.
- Boudra, D. B., and E. P. Chassignet, 1988: Dynamics of Agulhas retroflection and ring formation in a numerical model. Part I: The vorticity balance. *J. Phys. Oceanogr.*, **18**, 280–303.
- Bryan, F. O., C. W. Böning, and W. R. Holland, 1995: On the mid-latitude circulation in a high-resolution model of the North Atlantic. *J. Phys. Oceanogr.*, **25**, 289–305.
- Cessi, P., 1991: Laminar separation of colliding western boundary currents. *J. Mar. Res.*, **49**, 697–717.
- Chao, Y., A. Gangopadhyay, F. O. Bryan, and W. R. Holland, 1996: Modeling the Gulf Stream System: How far from reality? *Geophys. Res. Lett.*, **23**, 3155–3158.
- Chassignet, E. P., 1995: Vorticity dissipation by western boundary currents in the presence of outcropping layers. *J. Phys. Oceanogr.*, **25**, 242–255.
- , and P. R. Gent, 1991: The influence of boundary conditions on midlatitude jet separation in ocean numerical models. *J. Phys. Oceanogr.*, **21**, 1290–1299.
- , and R. Bleck, 1993: The influence of layer outcropping on the separation of boundary currents. Part I: The wind-driven experiments. *J. Phys. Oceanogr.*, **23**, 1485–1507.
- , —, and C. G. H. Rooth, 1995: The influence of layer outcropping on the separation of boundary currents. Part II: The wind- and buoyancy-driven experiments. *J. Phys. Oceanogr.*, **25**, 2404–2422.
- Dengg, J., 1993: The problem of Gulf Stream separation: A barotropic approach. *J. Phys. Oceanogr.*, **23**, 2182–2200.
- , A. Beckmann, and R. Gerdes, 1996: The Gulf Stream separation problem. *The Warmwatersphere of the North Atlantic Ocean*, W. Krauss, Ed., Gebr. Borntraeger, 253–290.
- Ezer, T., and G. Mellor, 1992: A numerical study of the variability and the separation of the Gulf Stream, induced by surface atmospheric forcing and lateral boundary flows. *J. Phys. Oceanogr.*, **22**, 660–682.
- Gazdag, J., 1976: Time-differencing schemes and transform methods. *J. Comput. Phys.*, **20**, 196–207.
- Greenspan, H. P., 1963: A note concerning topography and inertial currents. *J. Mar. Res.*, **21**, 147–154.
- Haidvogel, D. B., J. C. McWilliams, and P. R. Gent, 1991: Boundary current separation in a quasigeostrophic, eddy-resolving ocean circulation model. *J. Phys. Oceanogr.*, **22**, 882–902.
- Harrison, D. E., and W. R. Holland, 1981: Regional eddy vorticity transport and the equilibrium vorticity budgets of a numerical model ocean circulation. *J. Phys. Oceanogr.*, **11**, 190–208.
- Hellerman, S., and M. Rosenstein, 1983: Normal monthly wind stress over the world ocean with error estimates. *J. Phys. Oceanogr.*, **13**, 1093–1104.
- Hogg, N. G., and W. E. Johns, 1995: Western boundary currents. *Rev. Geophys.*, **33**(Suppl.), 1311–1334.
- , R. S. Pickart, R. M. Hendry, and W. J. Smethie Jr., 1986: The northern recirculation gyre of the Gulf Stream. *Deep-Sea Res.*, **33**, 1139–1165.
- Holland, W. R., 1967: On the wind-driven circulation in an ocean with bottom topography. *Tellus*, **19**, 582–600.
- , 1973: Baroclinic and topographic influences on the transport in western boundary currents. *Geophys. Fluid Dyn.*, **4**, 187–210.
- , 1978: The role of mesoscale eddies in the general circulation of the ocean. *J. Phys. Oceanogr.*, **8**, 363–392.
- Holloway, G., 1992: Representing topographic stress for large-scale ocean models. *J. Phys. Oceanogr.*, **22**, 1033–1046.
- Hsiung, J., 1985: Estimates of global oceanic meridional heat transport. *J. Phys. Oceanogr.*, **15**, 1405–1413.
- Huang, R. X., and G. R. Flierl, 1987: Two-layer models for the thermocline and current structure in the subtropical/subpolar gyres. *J. Phys. Oceanogr.*, **17**, 872–884.
- Isemer, H. J., and L. Hasse, 1987: *The Bunker Climate Atlas of the North Atlantic Ocean*. Vol. 2, *Air-Sea Interactions*, Springer-Verlag, 252 pp.
- Leetmaa, A., and A. F. Bunker, 1978: Updated charts of the mean annual wind stress, convergences in the Ekman layers, and the Sverdrup transports in the North Atlantic. *J. Mar. Res.*, **36**, 311–322.
- Mayer, D. A., and R. H. Weisberg, 1993: A description of COADS surface meteorological fields and implied Sverdrup transports for the Atlantic Ocean from 30°S to 60°N. *J. Phys. Oceanogr.*, **23**, 2201–2221.
- Mertz, G., and D. G. Wright, 1992: Interpretations of the JEBAR term. *J. Phys. Oceanogr.*, **22**, 301–305.
- Munk, W. H., 1950: On the wind-driven ocean circulation. *J. Meteor.*, **7**, 79–93.
- Myers, P. G., A. F. Fanning, and A. J. Weaver, 1996: JEBAR, pressure torque and Gulf Stream separation. *J. Phys. Oceanogr.*, **26**, 671–683.
- Parsons, A. T., 1969: A two-layer model of Gulf Stream separation. *J. Fluid Mech.*, **39**, 511–528.
- Salmon, R., 1992: A two-layer Gulf Stream over a continental slope. *J. Mar. Res.*, **50**, 341–365.
- , 1994: Generalized two-layer models of ocean circulation. *J. Mar. Res.*, **52**, 865–908.
- Schmitz, W. J., Jr., and W. S. Richardson, 1968: On the transport of the Florida Current. *Deep-Sea Res.*, **15**, 679–693.
- Spall, M. A., 1996: Dynamics of the Gulf Stream/deep western boundary current crossover. Part I: Entrainment and recirculation. *J. Phys. Oceanogr.*, **26**, 2152–2168.
- Stommel, H., 1948: The westward intensification of wind-driven ocean currents. *Trans. Amer. Geophys. Union*, **19**, 202–206.
- , 1965: *The Gulf Stream: A Physical and Dynamical Description*. 2d ed. University of California Press, 248 pp.
- Thompson, L., 1995: The effect of continental rises on the wind-driven ocean circulation. *J. Phys. Oceanogr.*, **15**, 1296–1316.
- , and W. J. Schmitz Jr., 1989: A limited-area model of the Gulf Stream: Design, initial experiments, and model–data intercomparison. *J. Phys. Oceanogr.*, **19**, 791–814.
- Veronis, G., 1973: Model of World Ocean circulation. Part I: Wind-driven, two-layer. *J. Mar. Res.*, **31**, 228–288.
- Verron, J., and E. Blayo, 1996: The no-slip condition and the separation of western boundary currents. *J. Phys. Oceanogr.*, **26**, 1938–1951.
- Warren, B. A., 1963: Topographic influences on the path of the Gulf Stream. *Tellus*, **15**, 167–183.
- Weatherly, G. L., 1984: An estimate of bottom frictional dissipation by Gulf Stream fluctuations. *J. Mar. Res.*, **42**, 289–301.
- Woods, L. C., 1954: A note on the numerical solution of fourth order differential equations. *Aeronaut. Quart.*, **5**(3), 575–583.